ISSN
2395-6992

International Journal of Engineering Research & Science

www.ijoer.com
www.adpublications.org

Volume-10! Issue-1! January, 2024 www.ijoer.com ! info@ijoer.com

Preface

We would like to present, with great pleasure, the inaugural volume-10, Issue-1, January 2024, of a scholarly journal, *International Journal of Engineering Research & Science*. This journal is part of the AD Publications series *in the field of Engineering, Mathematics, Physics, Chemistry and science Research Development*, and is devoted to the gamut of Engineering and Science issues, from theoretical aspects to application-dependent studies and the validation of emerging technologies.

This journal was envisioned and founded to represent the growing needs of Engineering and Science as an emerging and increasingly vital field, now widely recognized as an integral part of scientific and technical investigations. Its mission is to become a voice of the Engineering and Science community, addressing researchers and practitioners in below areas:

Chemical Engineering	
Biomolecular Engineering	Materials Engineering
Molecular Engineering	Process Engineering
Corrosion Engineering	
Civil Engineering	
Environmental Engineering	Geotechnical Engineering
Structural Engineering	Mining Engineering
Transport Engineering	Water resources Engineering
Electrical Engineering	
Power System Engineering	Optical Engineering
Mechanical Engineering	
Acoustical Engineering	Manufacturing Engineering
Optomechanical Engineering	Thermal Engineering
Power plant Engineering	Energy Engineering
Sports Engineering	Vehicle Engineering
Software Engineering	
Computer-aided Engineering	Cryptographic Engineering
Teletraffic Engineering	Web Engineering
System Engineering	
Mathematics	
Arithmetic	Algebra
Number theory	Field theory and polynomials
Analysis	Combinatorics
Geometry and topology	Topology
Probability and Statistics	Computational Science
Physical Science	Operational Research
Physics	
Nuclear and particle physics	Atomic, molecular, and optical physics
Condensed matter physics	Astrophysics
Applied Physics	Modern physics
Philosophy	Core theories

Chemistry	
Analytical chemistry	Biochemistry
Inorganic chemistry	Materials chemistry
Neurochemistry	Nuclear chemistry
Organic chemistry	Physical chemistry
Other Engineering Areas	
Aerospace Engineering	Agricultural Engineering
Applied Engineering	Biomedical Engineering
Biological Engineering	Building services Engineering
Energy Engineering	Railway Engineering
Industrial Engineering	Mechatronics Engineering
Management Engineering	Military Engineering
Petroleum Engineering	Nuclear Engineering
Textile Engineering	Nano Engineering
Algorithm and Computational Complexity	Artificial Intelligence
Electronics & Communication Engineering	Image Processing
Information Retrieval	Low Power VLSI Design
Neural Networks	Plastic Engineering

Each article in this issue provides an example of a concrete industrial application or a case study of the presented methodology to amplify the impact of the contribution. We are very thankful to everybody within that community who supported the idea of creating a new Research with IJOER. We are certain that this issue will be followed by many others, reporting new developments in the Engineering and Science field. This issue would not have been possible without the great support of the Reviewer, Editorial Board members and also with our Advisory Board Members, and we would like to express our sincere thanks to all of them. We would also like to express our gratitude to the editorial staff of AD Publications, who supported us at every stage of the project. It is our hope that this fine collection of articles will be a valuable resource for *IJOER* readers and will stimulate further research into the vibrant area of Engineering and Science Research.

Mukesh Arora

(Chief Editor)

Board Members

Dr. M. Varatha Vijayan

Annauniversity Rank Holder, Commissioned Officer Indian Navy, Ncc Navy Officer (Ex-Serviceman Navy), Best Researcher Awardee, Best Publication Awardee, Tamilnadu Best Innovation & Social Service Awardee From Lions Club.

Dr. Mohamed Abdel Fatah Ashabrawy Moustafa

PhD. in Computer Science - Faculty of Science - Suez Canal University University, 2010, Egypt.

Assistant Professor Computer Science, Prince Sattam bin AbdulAziz University ALkharj, KSA.

Prof.S.Balamurugan

Dr S. Balamurugan is the Head of Research and Development, Quants IS & CS, India. He has authored/co-authored 35 books, 200+ publications in various international journals and conferences and 6 patents to his credit. He was awarded with Three Post-Doctoral Degrees - Doctor of Science (D.Sc.) degree and Two Doctor of Letters (D.Litt) degrees for his significant contribution to research and development in Engineering.

Dr. Mahdi Hosseini

Dr. Mahdi did his Pre-University (12^{th}) in Mathematical Science. Later he received his Bachelor of Engineering with Distinction in Civil Engineering and later he Received both M.Tech. and Ph.D. Degree in Structural Engineering with Grade "A" First Class with Distinction.

Dr. Anil Lamba

Practice Head – Cyber Security, EXL Services Inc., New Jersey USA.

Dr. Anil Lamba is a researcher, an innovator, and an influencer with proven success in spearheading Strategic Information Security Initiatives and Large-scale IT Infrastructure projects across industry verticals. He has helped bring about a profound shift in cybersecurity defense. Throughout his career, he has parlayed his extensive background in security and a deep knowledge to help organizations build and implement strategic cybersecurity solutions. His published researches and conference papers has led to many thought provoking examples for augmenting better security.

Dr. Ali İhsan KAYA

Currently working as Associate Professor in Mehmet Akif Ersoy University, Turkey.

Research Area: Civil Engineering - Building Material - Insulation Materials Applications, Chemistry - Physical Chemistry – Composites.

Dr. Parsa Heydarpour

Ph.D. in Structural Engineering from George Washington University (Jan 2018), GPA=4.00.

Dr. Heba Mahmoud Mohamed Afify

Ph.D degree of philosophy in Biomedical Engineering, Cairo University, Egypt worked as Assistant Professor at MTI University.

Dr. Aurora Angela Pisano

Ph.D. in Civil Engineering, Currently Serving as Associate Professor of Solid and Structural Mechanics (scientific discipline area nationally denoted as ICAR/08"–"Scienza delle Costruzioni"), University Mediterranea of Reggio Calabria, Italy.

Dr. Faizullah Mahar

Associate Professor in Department of Electrical Engineering, Balochistan University Engineering & Technology Khuzdar. He is PhD (Electronic Engineering) from IQRA University, Defense View, Karachi, Pakistan.

Prof. Viviane Barrozo da Silva

Graduated in Physics from the Federal University of Paraná (1997), graduated in Electrical Engineering from the Federal University of Rio Grande do Sul - UFRGS (2008), and master's degree in Physics from the Federal University of Rio Grande do Sul (2001).

Dr. S. Kannadhasan

Ph.D (Smart Antennas), M.E (Communication Systems), M.B.A (Human Resources).

Dr. Christo Ananth

Ph.D. Co-operative Networks, M.E. Applied Electronics, B.E Electronics & Communication Engineering Working as Associate Professor, Lecturer and Faculty Advisor/ Department of Electronics & Communication Engineering in Francis Xavier Engineering College, Tirunelveli.

Dr. S.R.Boselin Prabhu

Ph.D, Wireless Sensor Networks, M.E. Network Engineering, Excellent Professional Achievement Award Winner from Society of Professional Engineers Biography Included in Marquis Who's Who in the World (Academic Year 2015 and 2016). Currently Serving as Assistant Professor in the department of ECE in SVS College of Engineering, Coimbatore.

Dr. PAUL P MATHAI

Dr. Paul P Mathai received his Bachelor's degree in Computer Science and Engineering from University of Madras, India. Then he obtained his Master's degree in Computer and Information Technology from Manonmanium Sundaranar University, India. In 2018, he received his Doctor of Philosophy in Computer Science and Engineering from Noorul Islam Centre for Higher Education, Kanyakumari, India.

Dr. M. Ramesh Kumar

Ph.D (Computer Science and Engineering), M.E (Computer Science and Engineering).

Currently working as Associate Professor in VSB College of Engineering Technical Campus, Coimbatore.

Dr. Maheshwar Shrestha

Postdoctoral Research Fellow in DEPT. OF ELE ENGG & COMP SCI, SDSU, Brookings, SD Ph.D, M.Sc. in Electrical Engineering from SOUTH DAKOTA STATE UNIVERSITY, Brookings, SD.

Dr. D. Amaranatha Reddy

Ph.D. (Postdocteral Fellow, Pusan National University, South Korea), M.Sc., B.Sc. : Physics.

Dr. Dibya Prakash Rai

Post Doctoral Fellow (PDF), M.Sc., B.Sc., Working as Assistant Professor in Department of Physics in Pachhuncga University College, Mizoram, India.

Dr. Pankaj Kumar Pal

Ph.D R/S, ECE Deptt., IIT-Roorkee.

Dr. P. Thangam

PhD in Information & Communication Engineering, ME (CSE), BE (Computer Hardware & Software), currently serving as Associate Professor in the Department of Computer Science and Engineering of Coimbatore Institute of Engineering and Technology.

Dr. Pradeep K. Sharma

PhD., M.Phil, M.Sc, B.Sc, in Physics, MBA in System Management, Presently working as Provost and Associate Professor & Head of Department for Physics in University of Engineering & Management, Jaipur.

Dr. R. Devi Priya

Ph.D (CSE), Anna University Chennai in 2013, M.E, B.E (CSE) from Kongu Engineering College, currently working in the Department of Computer Science and Engineering in Kongu Engineering College, Tamil Nadu, India.

Dr. Sandeep

Post-doctoral fellow, Principal Investigator, Young Scientist Scheme Project (DST-SERB), Department of Physics, Mizoram University, Aizawl Mizoram, India- 796001.

Dr. Roberto Volpe

Faculty of Engineering and Architecture, Università degli Studi di Enna "Kore", Cittadella Universitaria, 94100 – Enna (IT).

Dr. S. Kannadhasan

Ph.D (Smart Antennas), M.E (Communication Systems), M.B.A (Human Resources).

Research Area: Engineering Physics, Electromagnetic Field Theory, Electronic Material and Processes, Wireless Communications.

Mr. Amit Kumar

Amit Kumar is associated as a Researcher with the Department of Computer Science, College of Information Science and Technology, Nanjing Forestry University, Nanjing, China since 2009. He is working as a State Representative (HP), Spoken Tutorial Project, IIT Bombay promoting and integrating ICT in Literacy through Free and Open Source Software under National Mission on Education through ICT (NMEICT) of MHRD, Govt. of India; in the state of Himachal Pradesh, India.

Mr. Tanvir Singh

Tanvir Singh is acting as Outreach Officer (Punjab and J&K) for MHRD Govt. of India Project: Spoken Tutorial - IIT Bombay fostering IT Literacy through Open Source Technology under National Mission on Education through ICT (NMEICT). He is also acting as Research Associate since 2010 with Nanjing Forestry University, Nanjing, Jiangsu, China in the field of Social and Environmental Sustainability.

Mr. Abilash

MTech in VLSI, BTech in Electronics & Telecommunication engineering through A.M.I.E.T.E from Central Electronics Engineering Research Institute (C.E.E.R.I) Pilani, Industrial Electronics from ATI-EPI Hyderabad, IEEE course in Mechatronics, CSHAM from Birla Institute Of Professional Studies.

Mr. Varun Shukla

M.Tech in ECE from RGPV (Awarded with silver Medal By President of India), Assistant Professor, Dept. of ECE, PSIT, Kanpur.

Mr. Shrikant Harle

Presently working as a Assistant Professor in Civil Engineering field of Prof. Ram Meghe College of Engineering and Management, Amravati. He was Senior Design Engineer (Larsen & Toubro Limited, India).

Zairi Ismael Rizman

Senior Lecturer, Faculty of Electrical Engineering, Universiti Teknologi MARA (UiTM) (Terengganu) Malaysia Master (Science) in Microelectronics (2005), Universiti Kebangsaan Malaysia (UKM), Malaysia. Bachelor (Hons.) and Diploma in Electrical Engineering (Communication) (2002), UiTM Shah Alam, Malaysia.

Mr. Ronak

Qualification: M.Tech. in Mechanical Engineering (CAD/CAM), B.E.

Presently working as a Assistant Professor in Mechanical Engineering in ITM Vocational University, Vadodara. Mr. Ronak also worked as Design Engineer at Finstern Engineering Private Limited, Makarpura, Vadodara.

Table of Contents

Volume-10, Issue-1, January 2024

Prediction of Effective Drug Combinations based on Potential Drug Profiles

Changheng Li*

College of Big Data Statistics, Guizhou University of Finance and Economics, Guiyang, China
*Corresponding Author

Received: 01 January 2024/ Revised: 11 January 2024/ Accepted: 18 January 2024/ Published: 31-01-2024

Abstract— *Cancer is a great threat to the health of all mankind, and cancer monotherapy has been characterized by drawbacks such as toxicity and drug resistance. With the development of network pharmacology, multi-targeted drug combinations have become an ideal choice for cancer treatment. The dosage of combination drugs is usually lower than that of monotherapies, which has the advantages of improving efficacy, reducing toxicity, and delaying the development of drug resistance. In order to obtain better prediction results, this paper proposes a method for constructing drug potential features based on graph embedding model to predict anticancer drug combinations, establishes a control group to validate our method, and selects four performance metrics to measure the prediction performance of the model. The results show that the prediction results obtained from the drug potential features are better than the drug features. The drug potential features we designed can be used as one of the optional features for predicting drug combinations.*

Keywords— synergistic drug combinations, graph embedding, machine learning, cancer, neural network.

I. INTRODUCTION

Chemotherapy is a commonly used treatment for cancer, which often has many side effects, such as drug resistance and toxicity. With the development of modern medicine, drug combinations have become an ideal method for cancer treatment. By combining two or more anticancer drugs, drug toxicity can be reduced, drug resistance can be delayed, and efficacy can be improved. Therefore, finding synergistic combinations of drugs for specific cancer types is important to improve the efficacy of anticancer therapy[1-3].

Methods such as machine learning models offer the possibility to explore the combination space effectively. Machine learning models can quickly adapt to the ever-changing task of anticancer drug combination prediction and continuously optimize the prediction results. For example, by using machine learning models such as support vector machines, random forests, and neural networks, synergistic effects between different drugs can be effectively predicted[2, 4, 5].

In recent years, various prediction methods for anticancer drug combinations have been developed rapidly, e.g., Li et al [6]proposed a novel network propagation method based on gene-gene networks and drug-target information to simulate molecular signatures after treatment. By comparing the models of individual features, it was found that single-drug treatment data were better predictors of drug synergism than simulated molecular profiles. Janizek et al[7] predicted drug synergism using the physicochemical properties of the drug and the gene expression level of the cell line based on the XGBoost, and the results showed that 83 out of the 100 features with the highest level of evaluation were drug-based, which suggests that in the importance of drug features is higher than that of cell line features in the experiments for predicting drug combinations. Recently, Wang et al[8] proposed a new deep learning prediction model, PRODeepSyn. The model utilizes graph convolutional neural networks to integrate protein-protein interaction networks (PPIs) and histological data to construct low-dimensional embeddings of cell lines, and then constructs feed-forward neural networks with a batch normalization mechanism to compute drug synergy scores. In addition, Hu et al[9] understood the mechanism of drug synergism from the perspective of chemical-gene-tissue interactions and proposed a DTSyn model based on the mechanism of multiple attention to identify new drug

combinations, and they designed a fine-grained transformer encoder to capture chemical substructure-gene and gene-gene associations as well as a coarse-grained transformer encoder to extract chemical-chemical and chemical-cell lineage interactions, and finally designed a multilayer perceptron (MLP) to predict new drug combinations by connecting the outputs of the two transformer encoders in series as inputs to the MLP.

By summarizing the previous research, this paper understands that drug features are more important than cell line features in the experiments of predicting drug combinations, but through the research of the above scholars, there are few innovative studies on drug features, this paper constructs a set of potential features of drugs by using the graph embedding model, and puts forward a new method of predicting synergistic effects of anticancer drugs based on the constructing of potential features of drugs by the graph embedding model.

II. FEATURE ENGINEERING

2.1 Data set:

NCI-ALMANAC(National Cancer Institute - Analysis of Large-Scale Molecular Cancer Pharmacogenomic Data) is a publicly available database developed by the National Cancer Institute (NCI) to improve cancer therapeutic outcomes by identifying effective drug combinations and predicting patient response[10]. NCI-ALMANAC contains data on more than 60 cancer cell lines and more than 100 drugs, including FDA-approved drugs and experimental compounds. In this paper, we use the NCI-ALMANAC dataset as a source of anticancer drug synergy prediction data. In NCI-ALMANAC, the combinatorial effects of drugs are quantified by a method called ComboScore (a modified version of the Bliss independence model). The theoretical expectation of the effect when the effect is additive is calculated from the entire dose-response matrix considering the effects achieved by the combination of drug combinations, cell lineage metagenomes, and gains (or losses). Positive values of the ComboScore indicate that the drug combinations are synergistic, whereas negative values indicate that the drug combinations are not synergistic (those with purely additive effects obtain a ComboScore value of zero). In this paper, only drugs possessing at least one target gene were considered (68 drugs), and 59 cancer cell lines were selected through screening, with a total of 130,182 samples for model training and prediction. All NCI-60 cell line characteristics (expression, mutation, CNV, etc.) were downloaded from CellMinerCDB. Drug target information was obtained from DrugBank, and drug molecular properties were calculated using the RDKit package in Python.

2.2 Feature selection:

Gene expression profiling plays an important role in the prediction of anticancer drug combinations, and gene expression profiling can help reveal the mechanism of drug action on tumor cells. By analyzing the changes in gene expression profiles, the regulatory effects of certain anticancer drug combinations on specific signaling pathways, genes, or proteins can be understood, providing clues for understanding drug action. Referring to the studies of Janizek, RemziCelebi, and Preuer, et al [7, 11, 12], this paper decides to use the gene expression profiles as the cell lineage characteristics.

Morgan molecular fingerprints can be used to compare the similarities and correlations between different compounds, and by comparing the Morgan molecular fingerprints of anticancer drug molecules with those of other compounds, it is possible to predict possible interactions, including synergism, antagonism, etc., between them. Drug target information helps to better understand drug-target interactions. Monotherapy information may play an important role in anticancer drug combination prediction[6], and drug features may be more important than cell line features in prediction[7], In summary, in this paper, Morgan molecular fingerprints, drug target information, and monotherapy information are selected as drug features. In this paper, the selected drug features are utilized for comparison experiments with the designed drug potential features.

2.3 Machine learning and deep learning models:

2.3.1 CatBoost:

CatBoost is a gradient boosting tree framework with fewer parameters, support for categorical variables, and high accuracy, implemented as an oblivious trees-based learner. CatBoost uses ranked boosting to counteract noisy points in the training set, thus avoiding biased gradient estimation, and thus solving the prediction bias problem. CatBoost can match any state-of-the-art machine learning algorithm in terms of performance. rivals any state-of-the-art machine learning algorithm in that it reduces

the need for much hyper-parameter tuning, reduces the chance of overfitting, and makes the model more generalizable. In addition, CatBoost can handle categorical and numerical features and supports customized loss functions.

2.3.2 Deep Neural Network:

Feedforward Neural Network (FNN), also known as Multilayer Perceptron (MLP). It consists of multiple neurons and these neurons are arranged in a hierarchical structure. The basic structure of a feed forward neural network consists of an input layer, a hidden layer and an output layer. The input layer receives external input data, the hidden layer processes the data and extracts features, and the output layer performs classification or regression prediction based on the results of the hidden layer.

2.3.3 XGBoost:

XGBoost (eXtreme Gradient Boosting) is a machine learning algorithm based on gradient boosting decision trees. The core idea of XGBoost is to iteratively train weak classifiers (usually decision trees) and combine them into a powerful model. It employs gradient boosting to effectively optimize the objective function. Specifically, XGBoost improves the model's predictions incrementally by minimizing the negative gradient of the loss function. XGBoost performs well in all kinds of machine learning tasks, including classification, regression, and sorting.

2.3.4 Logistic Regression:

Logistic Regression is a statistical learning method for classification problems. It is a generalized linear model that makes classification decisions by mapping the output of a linear regression model to a probability value and using a logistic function. Logistic Sti regression assumes that there is a linear relationship between the dependent and independent variables and uses a logistic function (also known as a sigmoid function) to map the outcome of the linear combination to a probability between [0, 1], the sigmoid function formula is shown below:

$$P(y = 1|x) = \frac{1}{1+e^{-z}} \quad (1)$$

where $P(y = 1|x)$ denotes the probability that the dependent variable y takes the value 1 when the independent variable x is given, and z denotes the outcome of the linear combination. The training process of logistic Steele regression is to solve the parameters of the model by maximum likelihood estimation. Logistic Steele regression is widely used in practical applications, especially for binary classification problems, and is often used as a benchmark comparison for other machine learning algorithms.

III. CONSTRUCTION OF POTENTIAL DRUG FEATURES

In this paper, graph embedding model is utilized to construct drug based potential features. Graph embedding model is a technique for mapping nodes in a graph to a low-dimensional vector space, also known as graph representation learning. It converts high-dimensional graph data into a low-dimensional continuous vector representation by learning the relationships and features between nodes while preserving the original graph structure information.

Here, this paper proposes a network on drug-drug interaction. In this network, drugs are nodes and drug-drug interactions are edges. Considering that there are two kinds of drug-drug interactions, synergistic or antagonistic, a set of signed directed graphs is constructed, where "+" indicates that there is a synergistic interaction between two drugs and "-" idicates the existence of antagonism between two drugs. However, the effect of anticancer combination drugs can vary in different cell lines. This is because different cell lines have different genetic backgrounds, gene expression patterns, metabolic characteristics, etc., and thus the sensitivity and responsiveness to drugs will be different. Therefore, when constructing the drug-drug interaction network in this paper, cell lines need to be included in the consideration of the network.

In this paper the drug network contains three kinds of relationships, synergistic, antagonistic and unconnected edges, where synergistic represents a positive relationship and antagonistic represents a negative relationship. Referring to the study of Xu et al[13], for a given node pair (u, v), this paper calculates the inner product of U_u^{out}(positive outward vector) and U_v^{in} (positive received vector) and calls the result positive feedback F_{uv}^{+}, and calculates the inner product of W_u^{out} (negative outward vector) and W_v^{in} (negative received vector) and calls the result negative feedback F_{uv}^{-}. Next, this paper quantifies the effects of positive and negative feedback on the drug relationship with distributions denoted as $f_a(U_u^{out}U_v^{in})$and $f_a(W_u^{out}W_v^{in})$, where:

$$f_a(x) = \frac{p_0 e^x}{1+p_0(e^x-1)} \tag{2}$$

$f_a(x)$ is the activation function and $p_0$denotes the effect of no feedback. Next this paper defines the quantization of synergy, antagonism and zero as $F_{uv}^{+}(1-F_{uv}^{-})$, $(1-F_{uv}^{+})F_{uv}^{-}$ and $(1-F_{uv}^{+})(1-F_{uv}^{-})$,respectively. The node information in this paper is represented by four vectors, U_u^{out}, U_v^{in}, W_u^{out} and W_v^{in}, and the relationship from node u to v may contain synergism, antagonism and zero, which can be expressed as $f_a(U_u^{out}U_v^{in})\left(1-f_a(W_u^{out}W_v^{in})\right)$,$\left(1-f_a(U_u^{out}U_v^{in})\right)f_a(W_u^{out}W_v^{in})$ and $\left(1-f_a(U_u^{out}U_v^{in})\right)\left(1-f_a(W_u^{out}W_v^{in})\right)$.

In this paper, the negative log-likelihood loss function is chosen as the objective function, Negative Log-Likelihood Loss Function is a common loss function used in classification models, especially in logistic regression models are often used, Negative Log-Likelihood Loss Function has a lot of advantages in classification models. In order to relate the four vectors and the three drug relationships, the objective function is defined in this paper as the following equation:

$$L = -\sum_{(u,v)\in E^p}\log\left(F_{uv}^{+}(1-F_{uv}^{-})\right) - \sum_{(u,v)\in E^n}\log((1-F_{uv}^{+})F_{uv}^{-}) - \sum_{(u,v)\in E^{non}}\log\left((1-F_{uv}^{+})(1-F_{uv}^{-})\right) \tag{3}$$

Where E^p denotes the set of positively connected edges, E^n denotes the set of negatively connected edges, and E^{non} denotes the set of node pairs with no connected edges.

In order to minimize the objective function, this paper chooses gradient descent as the optimization function, which is a commonly used optimization algorithm to minimize the loss function and find the optimal parameters. The basic idea of gradient descent is to gradually reduce the value of the loss function by iteratively updating the parameters. Equation 3 consists of three components three components, the distribution for the synergistic, antagonistic and null relationships. In this paper, we use gradient descent to update the three vectors of one node in each iteration while fixing the vectors of all other nodes, so the problem becomes a convex optimization problem. The specific formulation is as follows:

$$L_{(u)} = -\sum_{v\in N_{out}^{p}(u)}\log\left(F_{uv}^{+}(1-F_{uv}^{-})\right) - \sum_{v\in N_{in}^{p}(u)}\log\left(F_{uv}^{+}(1-F_{uv}^{-})\right) - \sum_{v\in N_{out}^{n}(u)}\log((1-F_{uv}^{+})F_{uv}^{-}) - \sum_{v\in N_{in}^{n}(u)}\log((1-F_{uv}^{+})F_{uv}^{-}) - \sum_{v\in N_{out}^{non}(u)}\log\left((1-F_{uv}^{+})(1-F_{uv}^{-})\right) - \sum_{v\in N_{in}^{non}(u)}\log\left((1-F_{uv}^{+})(1-F_{uv}^{-})\right) \tag{4}$$

Where $N_{out}^{p}(u)$,$N_{out}^{n}(u)$,$N_{out}^{non}(u)$ denotes the set of three types of nodes with synergistic, antagonistic and zero relationships that node u outputs to node v. $N_{in}^{p}(u)$,$N_{in}^{n}(u)$,$N_{in}^{non}(u)$ denotes the set of three types of nodes with synergistic, antagonistic and zero relationships that node v inputs to u.

The dataset in this paper contains a total of 59 cell lines, which need to be divided into 59 copies, with each cell line corresponding to one copy of the dataset, which eliminates the interference of cell lines on the drug-drug interaction network. Next, the drug-drug interaction network needs to be established for each of these 59 copies of data. In this paper, the dimension of the potential features is set to be 16 dimensions, so the 16-dimensional potential features of each drug in the 59 cell lines are obtained. Since the data contained in these potential features are abstract and topological information of the network structure, it is difficult to capture the significance represented by each column, so this paper decided to merge the potential features of each drug in these 59 cell lines. Eventually, the dimension of the potential features for each drug is 944 dimensions, which is a 1 × 944 vector.

IV. PREDICTION RESULTS AND ANALYSIS

4.1 Experimental setup

In order to make the model generalizable to unseen datasets, this paper uses Stratified k-fold cross-validation to test the model. The advantage of stratified k-fold cross-validation is that it can better handle unbalanced datasets and ensure that the samples of each category are adequately represented during training and testing. This helps to reduce bias problems due to category imbalance and provides a more reliable assessment of model performance. Through stratified 5-fold cross-validation, this paper also adjusts the parameters of each model to obtain the optimal model.

Drug synergy prediction can be classified into two categories: regression task and classification task. In this paper, synergy prediction is considered as a classification task. Therefore, this paper chooses to binarize the synergy score, i.e., synergy is 1

and antagonism is 0. In this paper, the prediction thresholds of the models are optimized through hierarchical 5-fold cross validation to achieve the optimal equilibrium, and the final threshold is set to 10.

4.2 Comparison of predictive performance

In this paper, four performance metrics are used to measure the prediction performance of the model, which are the area under the receiver operating characteristic curve (ROC AUC), the area under the precision recall curve (PR AUC), the mean square error (MSE) and the Pearson correlation coefficient (PCC). The above performance metrics were calculated by five hierarchical cross-folding, and the average of the five results was taken as the final performance evaluation result. The predicted results are as follows:

TABLE 1
PERFORMANCE RESULTS OF FOUR MODELS (CELL LINE CHARACTERISTICS AND DRUG CHARACTERISTICS)

Model	ROC AUC	PR AUC	MSE	Pearson
CatBoost	0.9217	0.4651	0.1365	0.5335
Deep Neural Networks	0.9118	0.3876	0.1441	0.4761
XGBoost	0.8856	0.3601	0.1439	0.4552
Logistic Regression	0.8505	0.1945	0.1534	0.3101

TABLE 2
PERFORMANCE RESULTS OF FOUR MODELS (CELL LINE FEATURES AND DRUG POTENTIAL FEATURES)

Model	ROC AUC	PR AUC	MSE	Pearson
CatBoost	0.9258	0.4937	0.1348	0.5497
Deep Neural Networks	0.9178	0.4065	0.1459	0.4760
XGBoost	0.8943	0.3690	0.1430	0.4635
Logistic Regression	0.8657	0.2460	0.1507	0.3583

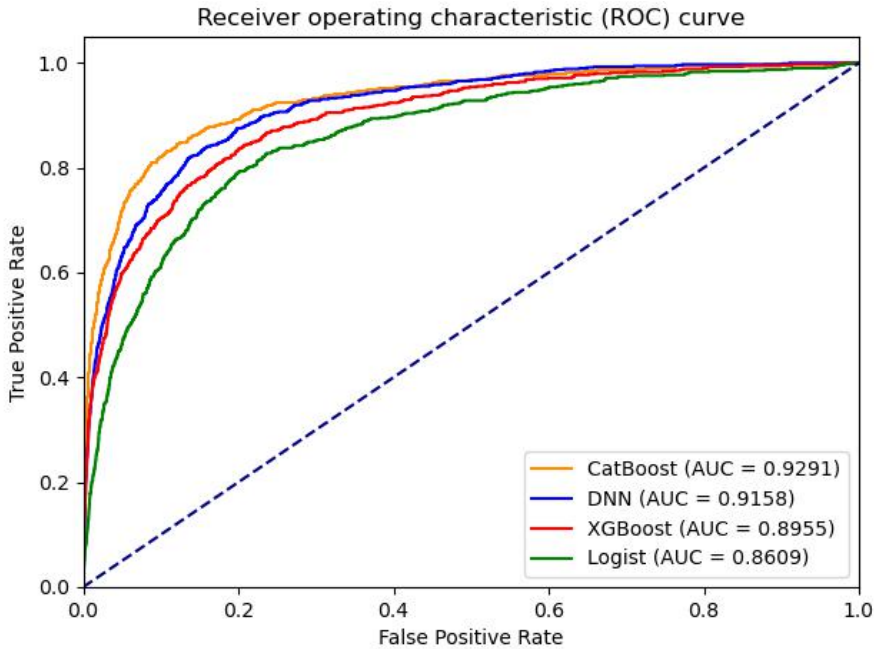

FIGURE 1: ROC curves of four models (cell line characteristics and drug characteristics)

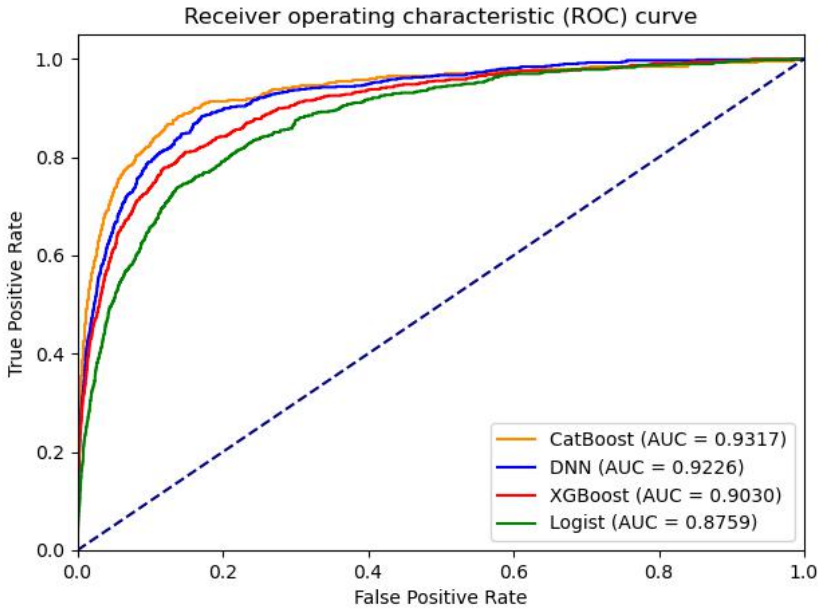

FIGURE 2: ROC curves of four models (cell line characteristics and drug potential characteristics)

Since Morgan molecular fingerprints, drug target information and monotherapy information have been outstanding in drug combination prediction, this paper firstly selects these three features together with cell line gene expression profiles as input features, and then utilizes popular machine learning algorithms for prediction respectively. Using different models for prediction and comparing the performance indexes of the above evaluated models, CatBoost, Deep Neural Networks, XGBoost and Logistic Regression algorithms finally show good prediction effects. The specific indexes are shown in Table 1, and the ROC curve is shown in Figure 1. Afterwards, in order to reflect the role of potential features of drugs in predicting effective drug combinations, this paper utilizes the potential features of drugs designed by the graph embedding model to replace the drug features to join, keep the parameters unchanged, and then carry out the same operation as above, and then the obtained indicators are shown in Table 2, and the ROC curves are shown in Fig. 2.

4.3 Result analysis

From the comparison of Tables 1 and 2, it can be seen that CatBoost and Deep Neural Networks have the best prediction effect, while XGBoost and Logistic Regression have poorer prediction effect when using cell line features and drug features for prediction. After using cell line features and drug potential features for prediction, the performance of the quasi-four models are improved to different degrees. In the case of ROC AUC, XGBoost and Logistic Regression improved more significantly, by 0.0087 and 0.0179, respectively. In the PR AUC, CatBoost and Logistic Regression are improved by 0.0283 and 0.0515 respectively, and in the MSE, CatBoost and Logistic Regression are reduced by 0.0087 and 0.0179 respectively. In the item of PCC, CatBoost and Logistic Regression improved more obviously. In summary, the drug potential features proposed in this paper are significantly better than the drug features and can be used as one of the optional features for predicting drug combinations.

V. CONCLUSION

The use of combinatorial drugs can undoubtedly help people to treat complex diseases, while the use of computer technology, histology and network technology helps people to discover new drug combinations and is therefore a proven means. The method greatly reduces the scope of the search and is safer and more reliable in a small area before experimental tests are carried out. Discovering new reliable features is also one of the keys to accurate prediction, and the drug potential features designed in this paper play an important role in improving the prediction accuracy, and among the four models, the contribution of drug potential features to the prediction accuracy is significantly higher than that of drug features. The Morgan molecular fingerprints, drug target information and monotherapy information used in this paper are basically classical and have been used by previous authors, so their credibility can be guaranteed.

The principle of constructing drug potential features in this paper lies in the need for a large amount of drug synergy information, and the accuracy can be further increased if enough drug synergy information is available. In addition, the drug

potential features constructed in this paper can also be utilized in the migration learning method, using a large number of drug-drug interactions in the data set, to extract the potential information to construct drug potential features, which can be applied to other prediction tasks that lack cell line information or drug feature information, which is also one of the future research directions. Finally, the models used in this paper are supervised models, and it is believed that the prediction accuracy will be further improved if semi-supervised models or other more advanced algorithms are utilized.

REFERENCES

[1] G. Chevereau and T. Bollenbach, "Systematic discovery of drug interaction mechanisms," *Molecular systems biology,* vol. 11, no. 4, p. 807, 2015.

[2] J. Jia *et al.*, "Mechanisms of drug combinations: interaction and network perspectives," *Nature Reviews Drug Discovery,* 2009.

[3] P. Csermely, T. Korcsmáros, H. J. M. Kiss, G. London, and R. Nussinov, "Structure and dynamics of molecular networks: A novel paradigm of drug discovery. A comprehensive review," *Pharmacology & therapeutics,* vol. 138, no. 3, pp. 333-408, 2013.

[4] L. He *et al.*, "Methods for High-Throughput Drug Combination Screening and Synergy Scoring," *Cold Spring Harbor Laboratory,* 2016.

[5] J. O'Neil *et al.*, "An unbiased oncology compound screen to identify novel combination strategies," *Molecular cancer therapeutics,* vol. 15, no. 6, pp. 1155-1162, 2016.

[6] H. Li, T. Li, D. Quang, and Y. Guan, "Network propagation predicts drug synergy in cancers," *Cancer research,* vol. 78, no. 18, pp. 5446-5457, 2018.

[7] J. D. Janizek, S. Celik, and S. I. Lee, "Explainable machine learning prediction of synergistic drug combinations for precision cancer medicine," *Cold Spring Harbor Laboratory,* 2018.

[8] X. Wang *et al.*, "PRODeepSyn: predicting anticancer synergistic drug combinations by embedding cell lines with protein–protein interaction network," *Briefings in Bioinformatics,* vol. 23, no. 2, p. bbab587, 2022.

[9] J. Hu *et al.*, "DTSyn: a dual-transformer-based neural network to predict synergistic drug combinations," *Briefings in Bioinformatics,* vol. 23, no. 5, p. bbac302, 2022.

[10] S. L. Holbeck *et al.*, "The National Cancer Institute ALMANAC: A Comprehensive Screening Resource for the Detection of Anticancer Drug Pairs with Enhanced Therapeutic Activity," *Cancer Research,* 2017.

[11] R. Celebi, O. Bear Don't Walk, R. Movva, S. Alpsoy, and M. Dumontier, "In-silico prediction of synergistic anti-cancer drug combinations using multi-omics data," *Scientific Reports,* vol. 9, no. 1, pp. 1-10, 2019.

[12] K. Preuer, R. P. Lewis, S. Hochreiter, A. Bender, K. C. Bulusu, and G. Klambauer, "DeepSynergy: predicting anti-cancer drug synergy with Deep Learning," *Bioinformatics,* vol. 34, no. 9, pp. 1538-1546, 2018.

[13] P. Xu, W. Hu, J. Wu, and B. Du, "Link prediction with signed latent factors in signed social networks," in *Proceedings of the 25th acm sigkdd international conference on knowledge discovery & data mining*, 2019, pp. 1046-1054.

[14] CHEVEREAU G, BOLLENBACH T. Systematic discovery of drug interaction mechanisms [J]. Molecular systems biology, 2015, 11(4): 807.

[15] AMZALLAG A, RAMASWAMY S, BENES C H. Statistical assessment and visualization of synergies for large-scale sparse drug combination datasets [J]. BMC bioinformatics, 2019, 20(1): 1-15.

[16] LUKAČIŠIN M, BOLLENBACH T. Emergent gene expression responses to drug combinations predict higher-order drug interactions [J]. Cell Systems, 2019, 9(5): 423-33. e3.

[17] LAKHTAKIA R, BURNEY I. A historical tale of two Lymphomas: part II: non-Hodgkin lymphoma [J]. Sultan Qaboos University Medical Journal, 2015, 15(3): e317.

[18] PROPERZI M, MAGRO P, CASTELLI F, et al. Dolutegravir-rilpivirine: first 2-drug regimen for HIV-positive adults [J]. Expert Review of Anti-Infective Therapy, 2018, 16(12): 877-87.

[19] DAVIES G, BOEREE M, HERMANN D, et al. Accelerating the transition of new tuberculosis drug combinations from Phase II to Phase III trials: New technologies and innovative designs [J]. PLoS medicine, 2019, 16(7): e1002851.

[20] MENDEN M P, WANG D, MASON M J, et al. Community assessment to advance computational prediction of cancer drug combinations in a pharmacogenomic screen [J]. Nature communications, 2019, 10(1): 2674.

[21] YI L, ZHOU L, LUO J, et al. Circ-PTK2 promotes the proliferation and suppressed the apoptosis of acute myeloid leukemia cells through targeting miR-330-5p/FOXM1 axis [J]. 2021, 86: 102506.

[22] DUQUESNE J, BOUGET V, COURNEDE P H, et al. Machine learning identifies a profile of inadequate responder to methotrexate in rheumatoid arthritis [J]. Rheumatology, 2023, 62(7): 2402-9.

Open-Loop Observer Structure for Disturbance Compensation using Adaptive Robust Design

Chao-Yun Chen

Green Energy and Environment Research Laboratories, Industrial Technology Research Institute, Chung, Hsing Rd., Chutung, Hsinchu, Taiwan

Received: 04 January 2024/ Revised: 13 January 2024/ Accepted: 20 January 2024/ Published: 31-01-2024

Abstract— *High accuracy and stability are generally indispensable in industrial control applications of servomechanism. Many unavoidable factors negatively influence the control performance, such as modeling uncertainties. Therefore, this investigation is concerned with the disturbance compensation for the reduction of modeling uncertainty and proposes an adaptive open-loop observer in which the output of the actual plant can asymptotically converge to the output of the nominal plant by using the adaptive gain adjustment. The gain is bounded through the projection-type adaptive law. Furthermore, the backstepping algorithm enhances the robustness for the disturbance attenuation. Additionally, the velocity control of a motor is simulated to confirm the performance of the proposed approach, and the experiments of trajectory tracking on a two-link rotor manipulator is used to verify the ability of the proposed approach.*

Keywords— Open loop observer; projection type adaptive law; backsteppin.

I. INTRODUCTION

High accuracy and stability are generally indispensable in industrial control applications of servomechanism. Many unavoidable factors negatively influence the control performance in real-word applications, such as the modeling uncertainties and the external disturbance. Therefore, a disturbance compensation scheme is stipulated need to reduce ad-verse effects resulting from modeling uncertainty and external disturbance.

The disturbance observer (DOB) is a popular control scheme for disturbance estimation and attenuation in actual applications [1-8]. The conventional DOB design requires an in-verse nominal model and a low pass filter, and the disturbance can be accurately estimated within the bandwidth of the low pass filter [1, 2]. Furthermore, the Luenberger observer can be considered as a closed-loop observer structure, whose gain can be adopted to estimate the disturbance [3-5]. Additionally, the extended state observer regards the lumped disturbance as an augmented state and utilizes the Luenberger observer structure to estimate the lumped disturbance [6-8].

Even if a DOB-based controller provides excellent disturbance attenuation, the disturbance rejection performance of the DOB is constrained by the bandwidth of the low pass filter. Moreover, since Luenberger observer would feed the estimated disturbance back to the nominal plant, this method may reduce the accuracy of disturbance estimation. Significantly, the open loop disturbance observer avoids this problem, but has another inherent drawback, its performance depends strongly on the accuracy of system modeling. To solve this problem, this investigation develops an adaptive algorithm to improve the performance affected by the modeling uncertainty, the adaptive control is a popular approach for the modeling uncertainties in control application [9-11]. The proposed algorithm aims to ensure that the output of the actual plant asymptotically con-verges to the output of the nominal plant by using the adaptive gain adjustment, and the gain is bounded through the projection type adaptive law. Additionally, the backstepping algorithm is adopted to enhance robustness in the disturbance compensation. The study makes three contributions: (1) adaptive gain adjustment of the disturbance compensation is proposed to solve the modeling inaccuracy, and the stability and convergence have proved by Lyapunov theorem, and (2) the proposed adaptive open loop observer can effectively suppress the external disturbance in the absence of modeling uncertainties; (3) the backstepping algorithm is adopted to enhance the performance of the proposed approach. Additionally, the velocity control of a motor is used as a simulation example to describe the performance comparisons of the conventional DOB and the proposed approach,

and the experiment of the trajectory tracking task has been conducted to verify the abilities of the proposed approach. Simulation and experimental results show that the proposed approach exhibits satisfactory performance.

The rest of the paper is organized as follows. A brief review of the open-loop observer structure for disturbance compensation is provided in Section 2. The proposed adaptive robust design for open-loop observer are descripted in Section3. The simulation and experimental results are introduced in Section 4. Section 5 gives the conclusions.

II. BRIEF INTRODUCTION OF THE OPEN-LOOP OBSERVER FOR DISTURBANCE COMPENSATION

The disturbance compensation structure can be demonstrated in a physical system described by using an nth-order LTI state space equation as

$$\dot{x}(t) = Ax(t) + B(u(t) + u_d - \hat{u}_d)$$
$$y(t) = Cx(t) \tag{1}$$

where $x \in R^n$ denotes the state vector; $y \in R^{q\times 1}$ denotes the output vector; $u \in R^{p\times 1}$ denotes the control input vector; $u_d \in R^{p\times 1}$ denotes the unknown disturbance vector connected with the physical plant; $\hat{u}_d \in R^{p\times 1}$ denotes estimated disturbance; $A \in R^{n\times n}$ denotes the state matrix; $B \in R^{n\times p}$ denotes the input matrix, and $C \in R^{q\times n}$ denotes the output matrix.

The nominal plant of Eq. (1) can be expressed as

$$\dot{x}_r(t) = A_r x_r(t) + B_r u(t)$$
$$y_r(t) = Cx_r(t) \tag{2}$$

where $x_r \in R^n$ is the nominal state vector; $y_r \in R^{q\times 1}$ is the nominal output vector; $u \in R^{p\times 1}$ is the nominal control input; $A_r \in R^{n\times n}$ is the nominal state matrix, and $B_r \in R^{n\times p}$ is the nominal input matrix.

Fig. 1 shows the open-loop disturbance observer. To estimate the disturbance u_d without the modeling error (i.e. $A = A_r$ and $B = B_r$), the state error is defined as $x_e = x - x_r$, and the error dynamics equation can be expressed as

$$\dot{x}_e = \dot{x} - \dot{x}_r = Ax_e + B(u_d - \hat{u}_d) \tag{3}$$

where $\hat{u}_d$ denotes the disturbance estimation, which can be written as

$$\hat{u}_d = \Gamma(y - y_r) = \Gamma C x_e \tag{4}$$

where Γ indicates the compensation gain. According to (3) and (4), the disturbance u_d can be suppressed by specifying a suitable gain Γ. However, the modeling error (i.e. $A \neq A_r$ and $B \neq B_r$) can in practice influence the disturbance estimation accuracy $\hat{u}_d$ and state error x_e convergence, since the performance of the open-loop disturbance observer is based on that the system parameters are accurately known in advance. To improve the disturbance compensation capabilities of the open-loop disturbance observer, an adaptive algorithm is used for adaptive adjustment of the compensation gain Γ, which improves the performance of the open-loop disturbance observer in the presence of modeling inaccuracy.

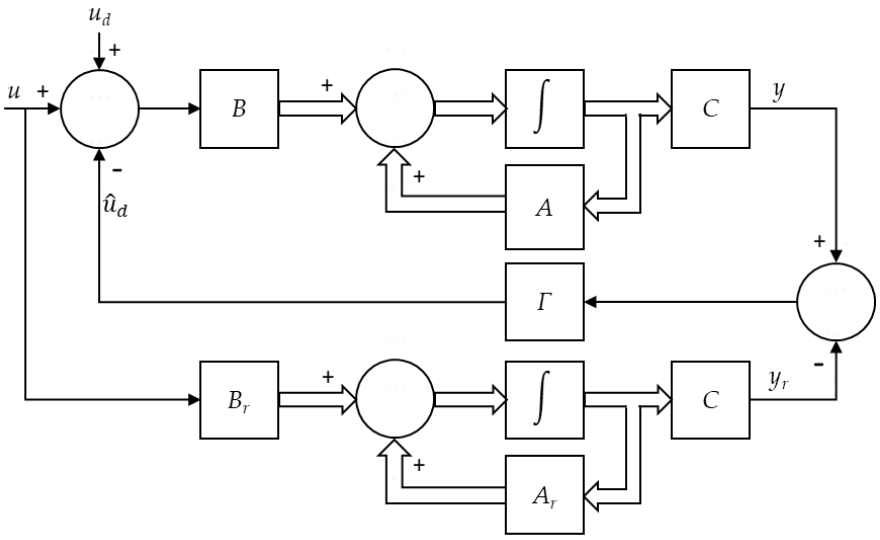

FIGURE 1: Open-Loop Disturbance Observer Structure for Disturbance Compensation

III. ADAPTIVE OPEN-LOOP DISTURBANCE OBSERVER

Considering the modeling inaccuracy, the error dynamic equation of (1) and (2) can be written as

$$\begin{aligned}\dot{x}_e &= Ax + B(u + u_d - \hat{u}_d) - A_r x_r - B_r \\ &= Ax + B(u + u_d - \hat{u}_d) - A_r x_r - B_r u + A_r x - A_r x + B_r(u_d - \hat{u}_d) - B_r(u_d - \hat{u}_d) \\ &= A_e x + A_r x_e + B_e(u + u_d - \hat{u}_d) + B_r u_d - B_r \hat{u}_d \end{aligned} \tag{5}$$

where$A_e = A - A_r$ and $B_e = B - B_r$ indicate the modeling error, and $\hat{u}_d$ can be chosen as follows:

$$\hat{u}_d = {B_r}^{-1}[A_e x + A_r x_e + B_e(u + u_d - \hat{u}_d) + B_r u_d - A_k x_e] \tag{6}$$

Notably, B_r is not a square matrix, therefore ${B_r}^{-1}$ represents the pseudo inverse matrix. If B_r has full row rank, then ${B_r}^{-1} = ({B_r}^T B_r)^{-1} {B_r}^T$. If B_r has full column rank, then ${B_r}^{-1} = {B_r}^T (B_r {B_r}^T)^{-1}$.

Substituting Eq. (6) into Eq. (5), the error dynamics equation can be rewritten as

$$\dot{x}_e = A_k x_e \tag{7}$$

where $A_k = \begin{bmatrix} 0 & 1 & 0 & \cdots & 0 \\ 0 & 0 & 1 & \cdots & 0 \\ \vdots & \vdots & \vdots & \cdots & \vdots \\ 0 & 0 & 0 & \cdots & 1 \\ -k_1 & -k_2 & -k_3 & \cdots & -k_n \end{bmatrix}$. Eq. (7) can be further described by

$$\begin{cases} \dot{x}_e^n = x_e^{n+1} \\ \dot{x}_e^{n+1} = \dot{x}_e^n + k_n x_e^n + k_{n-1} x_e^{n+1} + \cdots + k_1 x_e^1 \end{cases} \tag{8}$$

Eq. (8) indicates that $x_r(t) \rightarrow x(t)$ as $t \rightarrow \infty$, namely that the output error between y and y_r will asymptotically converge to zero.

Theoretically, Eq. (6) can completely eliminate the modeling error and the unknown external disturbance. However, since the modeling error and unknown external disturbance are very difficult to identify in advance, then Eq. (6) cannot be used in real application. If the objective of applying the open-loop disturbance observer is to ensure that the output error between y and y_r converges to zero, then an adaptive design can be adopted to formulate the disturbance compensation as Eq. (4) instead of Eq. (6). In the formulation proposed in Eq. (4), $\hat{u}_d$ can be further set as

$$\hat{u}_d(\Gamma, y_e) = \Gamma_{pid} E(y_e) \tag{9}$$

In Eq. (9), Γ_{pid} denotes the PID gain vector (Γ can be the Γ_p, Γ_{pi} or Γ_{pid} type depending on the application requirements) and $E(y_e)$ denotes the error vector which combines the proportional, integral and differential errors. In order to design PID gain of Γ_{pid} using the adaptive algorithm, the ideal disturbance compensation can be defined as

$$u_{ideal} = {B_r}^{-1}[A_e x + A_r x_e + B_e(u + u_d - \hat{u}_d) + B_r u_d - A_k x_e] \tag{10}$$

Adding and subtracting the $B_r u_{ideal}$ term to the right side of (5) leads to

$$\dot{x}_e = A_e x + A_r x_e + B_e(u + u_d - \hat{u}_d) + B_r u_d - B_r u_{ideal} + B_r(u_{ideal} - \hat{u}_d)$$

Substituting Eq. (10) into the fifth term on the right side of the above equation yields

$$\dot{x}_e = A_k x_e + B_r(u_{ideal} - \hat{u}_d) \tag{11}$$

Let the ${\Gamma^*}_{pid}$ be the optimal constant gain vector with a minimum error u_{er} between u_{ideal} and $\hat{u}_d$. Thus, ${\Gamma^*}_{pid}$can be defined as

$$\Gamma_{pid}^* = arg \;\; min_{\Gamma \in \Omega_\Gamma}\left[sup_{x \in \Omega_x}\left\|u_{ideal} - \hat{u}_d(\Gamma_{pid}, E)\right\|\right] \tag{12}$$

Based on Eq. (12), u_{er} can be defined as

$$u_{er} = u_{ideal} - \hat{u}_d(\Gamma_{pid}^*, E) \tag{13}$$

Moreover,

$$\hat{u}_d(\Gamma_{pid}, E) - \hat{u}_d(\Gamma_{pid}^*, E) = (\Gamma_{pid} - \Gamma_{pid}^*)E \tag{14}$$

according to Eqs. (11) and (13), the error dynamic equation can be rewritten as

$$\dot{x}_e = A_k x_e + B_r(\hat{u}_d(\Gamma_{pid}^*, E) - \hat{u}_d(\Gamma_{pid}, E) + u_{er}) = A_k x_e + B_r(u_{er} - (\Gamma_{pid} - \Gamma_{pid}^*)E) \quad (15)$$

Consider the Lyapunov function candidate $V(x_e(t))$

$$V(x_e(t)) = \frac{1}{2} {x_e}^T P x_e + \frac{1}{2}\eta^{-1}(\Gamma_{pid} - \Gamma_{pid}^*)^T(\Gamma_{pid} - \Gamma_{pid}^*) \quad (16)$$

where P is a positive definite symmetric matrix that satisfies the Lyapunov equation ${A_k}^T P + P A_k = -Q$, where Q is a given positive definite symmetric matrix with a minimum eigenvalue greater than 1, *i.e.* $\lambda_{min}(Q) > 1$, and η is an arbitrary constant. The time derivative of Eq. (16) can be expressed as

$$\begin{aligned} \dot{V}(x_e(t)) &= {x_e}^T P \dot{x}_e - \eta^{-1}(\Gamma_{pid} - \Gamma_{pid}^*)^T \dot{\Gamma} \\ &= -\frac{1}{2}{x_e}^T Q x_e + {x_e}^T P B_r u_{er} - \eta^{-1}(\Gamma_{pid} - \Gamma_{pid}^*)^T(\eta {x_e}^T P B_r E + \dot{\Gamma}_{pid}) \end{aligned} \quad (17)$$

According to Eq. (17), the gain Γ_{pid} is updated according to projection type parameter adaptation law [13]

$$\dot{\Gamma}_{pid} = \text{Proj}_{\Gamma}(-\eta {x_e}^T P B_r E) \quad (18)$$

where the projection mapping $\text{Proj}_{\Gamma}(-\eta {x_e}^T P B_r E)$ is defined as

$$\text{Proj}_{\Gamma}(-\eta {x_e}^T P B_r E) = \begin{cases} 0, & \text{if } \begin{cases} \Gamma_{pid} = \Gamma_{pid}^{max} \text{ and } -\eta {x_e}^T P B_r E > 0 \\ \Gamma_{pid} = \Gamma_{pid}^{min} \text{ and } -\eta {x_e}^T P B_r E < 0 \end{cases} \\ -\eta {x_e}^T P B_r E, & \text{otherwise} \end{cases} \quad (19)$$

Consequently, (18) becomes:

$$\dot{V}(x_e(t)) = -\frac{1}{2}{x_e}^T Q x_e + {x_e}^T P B_r u_{er} \le -\frac{1}{2}\lambda_{min}(Q)\|x_e\|^2 + \|x_e\|\|P B_r u_{er}\| \quad (20)$$

The stability of the proposed method of compensation gain tuning through a projection type parameter adaptation law is analyzed as described in [12], in which the Barbalat lemma was used to prove that $\lim_{t\to\infty}\|x_e(t)\| = 0$.

Remarks:

According to (20), assume that $\|u_{er}\| \le \varepsilon\|x_{er}\|$, where ε is an unknown positive constant. Eq. (20) can be rewritten as

$$\dot{V}(x_e(t)) \le -\frac{1}{2}\lambda_{min}(Q)\|x_e\|^2 + \varepsilon\|P B_r\|\|x_e\|^2 \quad (21)$$

From Eq. (21), if $\dot{V}(x_e(t)) \le 0$, which must satisfy the condition $\varepsilon \le \frac{1}{2}\frac{\lambda_{min}(Q)}{\|P B_r\|}$, which clearly indicates whether the norm of P is larger (*i.e.*, system robustness is increased). Additionally, η of Eq. (18) is used to determine the adjusted rate of Γ_{pid}. A larger η indicates a quicker adjusted rate. However, a high value for η may cause oscillation or instability. □

Although a suitable P and η can be chosen, the x_e asymptotically converges to zero. However, Eq. (16) is still subject to $u_{er} - (\Gamma_{pid} - \Gamma_{pid}^*)E$, *i.e.*, according to Eqs. (13) and (14), the ideal disturbance compensation can be expressed as

$$u_{ideal} = \hat{u}_d + u_{er} - (\Gamma_{pid} - \Gamma_{pid}^*)E = \hat{u}_d + u_{rc} \quad (22)$$

where $u_{rc} = u_{er} - (\Gamma_{pid} - \Gamma_{pid}^*)E$ is the approximation error for the disturbance estimation, and (15) can be rewritten as

$$\dot{x}_e = A_k x_e + B_r u_{rc} \quad (23)$$

Generally, many control applications calculate u_{rc} using the high gain technique. However, an appropriate high gain value for u_{rc} is hard to select in real-word applications. Therefore, this study adopted the backstepping algorithm presented in [13] to design u_{rc}. For a convenient description of the derivation of u_{rc}, let the nominal parameters B_r be the case where $B_r = [0 \quad 0 \quad \cdots \quad b] \in R^{n\times 1}$, Equation (23) can then be further written as

$$\dot{x}_e^{n+1} = -k_1 x_e^1 - k_2 x_e^2 - \cdots - k_n x_e^n + b u_{rc} \quad (24)$$

The new error variable is defined as

$$Z_{n+1} = x_{en+1} - \alpha_n \quad (25)$$

where α_n is the virtual control expressed as

$$\alpha_n = -c_n Z_n - Z_{n-1} + \dot{\alpha}_{n-1} \tag{26}$$

where c_n is the positive constant. The control Lyapunov function can thus be formulated as

$$V_{n+1} = \frac{1}{2}\sum_{i=1}^{n+1} Z_i^2 \tag{27}$$

and from (25) to (27), one can give

$$\dot{Z}_n = Z_{n+1} - c_n Z_n - Z_{n-1} \tag{28}$$

$$\dot{V}_{n+1} = -\sum_{i=1}^{n+1} Z_i^2 + Z_{n+1}(\dot{x}_e^{n+1} - \dot{\alpha}_n + Z_n) \tag{29}$$

which results in

$$\dot{Z}_{n+1} = -c_{n+1} Z_{n+1} - Z_n \tag{30}$$

$$\alpha_{n+1} = -c_{n+1} Z_{n+1} - Z_n + \dot{\alpha}_n \tag{31}$$

According to (24) to (31), u_{rc} can be chosen as

$$u_{rc} = b^{-1}[k_1 Z_1 + k_2(Z_2 + \alpha_1) + k_3(Z_3 + \alpha_2) + \cdots k_n(Z_n + \alpha_{n-1}) + \dot{\alpha}_n - Z_n] \tag{32}$$

Substituting the (32) into (29) yields

$$\dot{V}_{n+1} = -\sum_{i=1}^{n+1} Z_i^2 \tag{33}$$

Therefore, Eq. (27) is a positive definite; Eq. (33) is a semi-negative definite, and the new error variable Z_n can asymptotically converge to zero according to the Lyapunov stability theory [14]. Figure 2 is a block diagram of the adaptive open-loop disturbance observer.

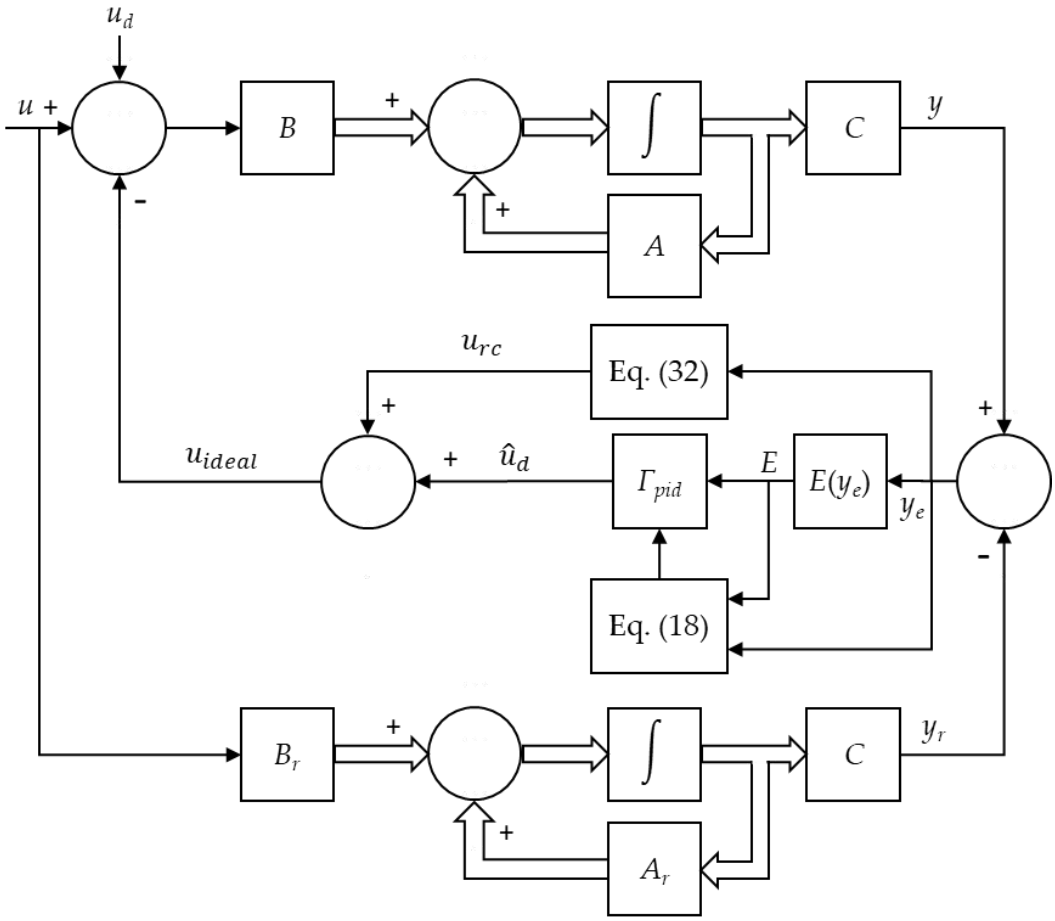

FIGURE 2: Adaptive Open Loop-Disturbance Observer

IV. SIMULATIONS AND EXPERIMENTS

This section may be divided by subheadings. It should provide a concise and precise description of the simulation and experimental results, their interpretations, as well as the conclusions that can be drawn.

4.1 Simulation results

To verify the proposed approach, a simulation was run using the constant velocity control of a motor as a potential application to compare the control performance of the proposed approach and the conventional DOB. The simulation software was MATLABR2014a.

The model parameters of the motor ware J=3.2964×10^{-4}Nm/(rad/s^2) and B=2.7312×10^{-4} Nm/(rad/s). The nominal models of DOB were set as J_{DOB}=2×10^{-4}Nm/(rad/s^2) for the DOB model J_n=2.747×10^{-4}Nm/(rad/s^2) and B_n=2.7312×10^{-4} Nm/(rad/s) . The PI controller was used as the feedback control, in which K_p=2 and K_i=0.8. The bandwidth of the low pass filter for the DOB was 100Hz. The parameter settings of the proposed approach were: $A_k = \begin{bmatrix} 0 & 1 \\ -2 & -10 \end{bmatrix}$ and Q = diag[4,4]. For the Lyapunov equation${A_k}^T P + PA_k = -Q$, $P = \begin{bmatrix} 10.6 & 1 \\ 1 & 0.3 \end{bmatrix}$. The definition of Γ_{pi} was $\Gamma_{pi} = [\Gamma_p \quad \Gamma_i]^T$; the upper and lower bounds of the gain matrix Γ_{pi} were $\Gamma_{pi}^{max} = [60 \quad 40]^T$ and $\Gamma_{pi}^{min} = [10 \quad 5]^T$, and the adaptation rate $\eta = 10$. According to Eq. (32), the u_{rc} can be designed as

$$u_{rc} = J_n[k_1 Z_1 + k_2(Z_2 + \alpha_1)] \tag{34}$$

where $Z_1 = x_{e1} = \theta - \theta_n$, $Z_2 = x_{e2} - c_1 Z_1 = \dot{x}_{e1} - c_1 Z_1$, and $\alpha_1 = -c_1 Z_1$. In these equations, θ denotes the rotation position of motor; θ_n denotes the rotation position of nominal plant, and $c_1 = 10$.

The time-varying external disturbance of 15sin(2πft) Nm is used in this simulation to verify the performance of the proposed approach. The frequency f had two cases, case1 10Hz and case2 80Hz.

Fig. 3 indicates the velocity response for case1 and case2. Clearly, the proposed approach performs better than the conventional DOB when the frequency of the external disturbance from low frequency becomes high frequency. Although the conventional DOB can increase the bandwidth of the low-pass filter, this method may increase noise levels, reducing the control performance in real applications.

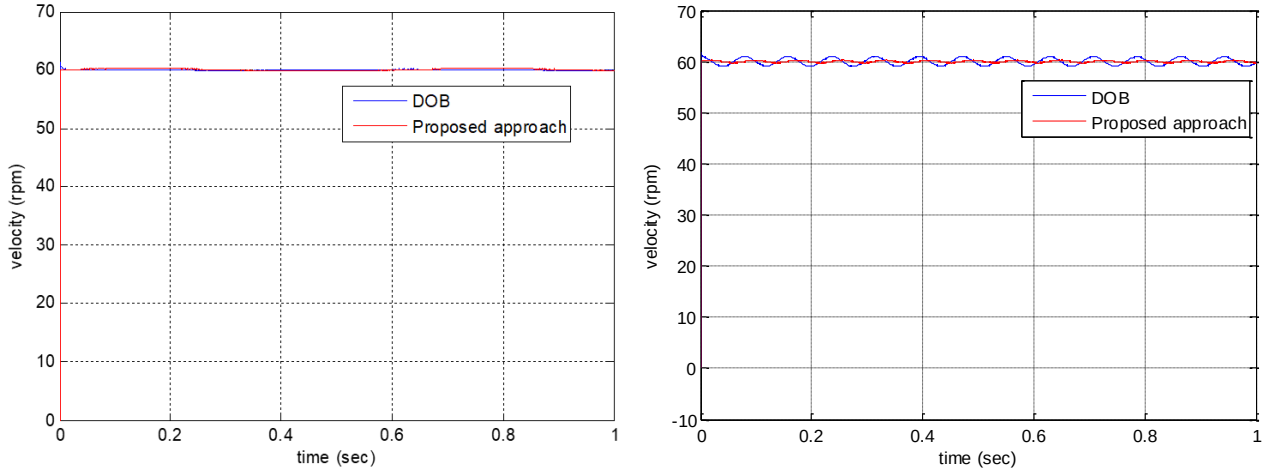

(a) (b)

FIGURE 3: Velocity Response (A) Case 1 (B) Case 2.

4.2 Experimental results

The circle-shaped trajectory tracking control experiment of the two-link rotor manipulator is aimed at evaluating the performances. The two-link robot manipulator is shown in Fig.4, which driven by two Panasonic AC servomotors (MHMD022S1S and MHMD042S1S), and a personal computer equipped with a motion control card (EPCIO-6000). Both servomotors have built-in incremental encoders (2500×4 pulses/rev) that can be used to provide position feedback. The parameters of the two-link robot manipulator are listed in TABLE 1.

FIGURE 4: Two-Link Robot Manipulator

TABLE 1
THE PARAMETERS OF THE TWO-LINK ROBOT MANIPULATOR

	Length	Mass	Center of Mass	Inertia
Link 1	0.24 m	2.35 kg	0.1557 m	0.01238 kgm2
Link 2	0.16 m	0.751kg	0.0981 m	0.00187 kgm2

In order to descript the modeling uncertainty suppression effect of the proposed approach, the controller of the two-link robot manipulator for the circle-shaped trajectory tracking has incorporated the friction compensation that worked the LuGre model [15], which can be described as follows:

$$\dot{z} = \dot{\theta} - \frac{\sigma_0|\dot{\theta}|}{s(\dot{\theta})}\mathrm{z} \tag{35}$$

$$\tau_f = \sigma_1\dot{z} + \sigma_0 z + \sigma_2\dot{\theta} \tag{36}$$

where z is the average deflection of the bristles between two contact surfaces, σ_0 is the stiffness which describes the relationship between displacement and friction in a reversal motion, σ_1 is the damping coefficient, σ_2 is the viscous coefficient, and $\mathrm{s}(\dot{\theta})$ is a nonlinear function used to describe the Stribeck effect. In [15], $\mathrm{s}(\dot{\theta})$ is expressed as

$$\mathrm{s}(\dot{\theta}) = F_c + (F_s - F_c)e^{-\alpha|\dot{\theta}|} \tag{37}$$

where F_c is the Coulomb friction, F_s is the stiction force, and α describes the variation of $\mathrm{s}(\dot{\theta})$ between F_s and F_c. The parameters of the LuGre friction model, i.e. σ_0, σ_1, σ_2, F_c, F_s, and α can be identified using the method proposed in [16]. The identified friction-velocity map of the two-link robot manipulator is shown in Fig. 5, and the obtained friction model parameters are listed in TABLE 2.

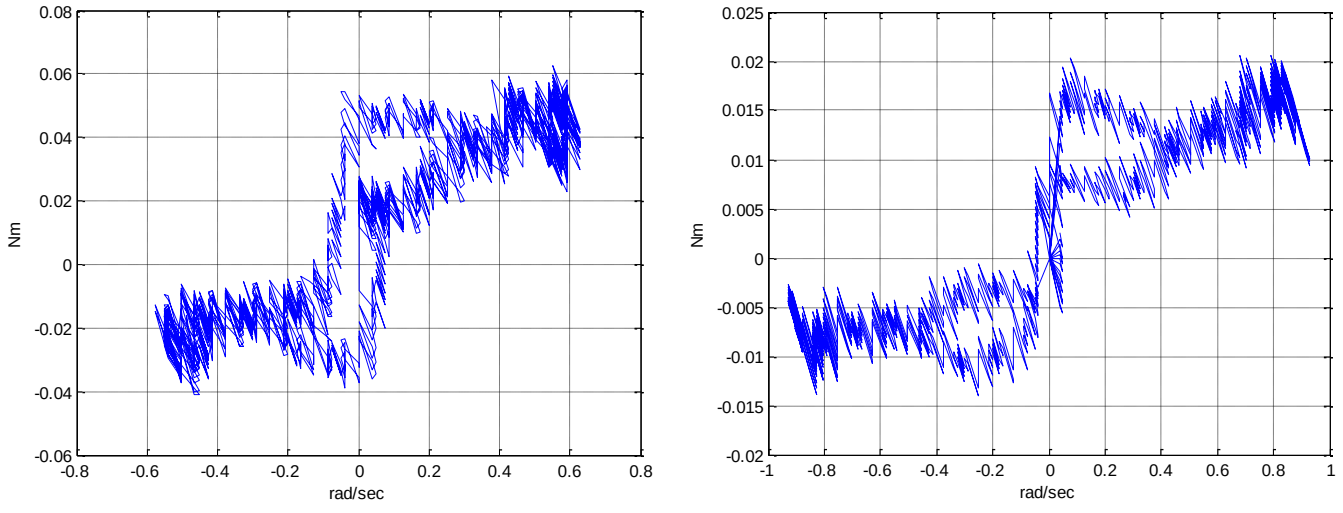

(a) (b)

FIGURE 5: Experimental Friction Velocity Map. (A) Joint 1 (B) Joint 2.

TABLE 2
FRICTION MODEL PARAMETERS OF THE TWO-LINK ROBOT MANIPULATOR

	σ_0(Nm/rad)	σ_1(Nm/rad/s)	σ_2(Nm/rad/s)	F_c(Nm)	F_s(Nm)	α
Joint1	0.18535	0.011494	0.00070987	0.044398	0.05078	0.11953
Joint2	0.11208	0.020577	0.00089763	0.022801	0.04575	0.05971

The parameter settings for the proposed approach are: $\eta = 100$, $A_k = \begin{bmatrix} 0_{2\times2} & I_{2*2} \\ K_1 & K_2 \end{bmatrix}$ and $Q = \text{diag}[50,50,50,50]$, where $K_1 = \begin{bmatrix} -0.5 & 0 \\ 0 & -0.5 \end{bmatrix}$ and $K_2 = \begin{bmatrix} -0.7 & 0 \\ 0 & -0.7 \end{bmatrix}$. For the Lyapunov equation ${A_k}^T P + P A_k = -Q$, $P = \begin{bmatrix} 88.57 & 0 & 50 & 0 \\ 0 & 88.57 & 0 & 50 \\ 50 & 0 & 107.14 & 0 \\ 0 & 50 & 0 & 107.14 \end{bmatrix}$ is used in the simulation. Moreover, since the two-link planar robot manipulator has two joints, it can be designed according to the definition of Γ_{pid} as $\Gamma_{pid} = [\Gamma_{p1} \quad \Gamma_{i1} \quad \Gamma_{d1} \quad \Gamma_{p2} \quad \Gamma_{i2} \quad \Gamma_{d2}]^T$, in which Γ_{p1}, Γ_{i1}, and Γ_{d1} are observer gain of joint1, moreover Γ_{p2}, Γ_{i2}, and Γ_{d2} are observer gain of joint2, the upper bound and lower bound of the Γ_{pid} are $\Gamma_{pid}^{max} = [60 \quad 30 \quad 50 \quad 50 \quad 20 \quad 40]^T$ and $\Gamma_{pid}^{min} = [20 \quad 6 \quad 10 \quad 10 \quad 5 \quad 4]^T$, respectively. The adaptation rate $\eta = 100$. According to (32), the approximation error u_{rc} for the disturbance estimation can be described in

$$u_{rc} = M_r[K_1 Z_1 + K_2(Z_2 + \alpha_1)] \tag{33}$$

where M_r is the inertia matrix of the nominal plant of the two-link planar robot manipulator, $Z_1 = x_{e1} = [q_1 - q_{r1} \quad q_2 - q_{r2}]^T$, $Z_2 = x_{e2} - c_1 Z_1 = \dot{x}_{e1} - c_1 Z_1$, and $\alpha_1 = -c_1 Z_1$, in which q_1 and q_2 are the joint angle of the robot manipulators, q_{r1} and q_{r2} are the joint angle of the nominal plant, and $c_1 = 0.3$.

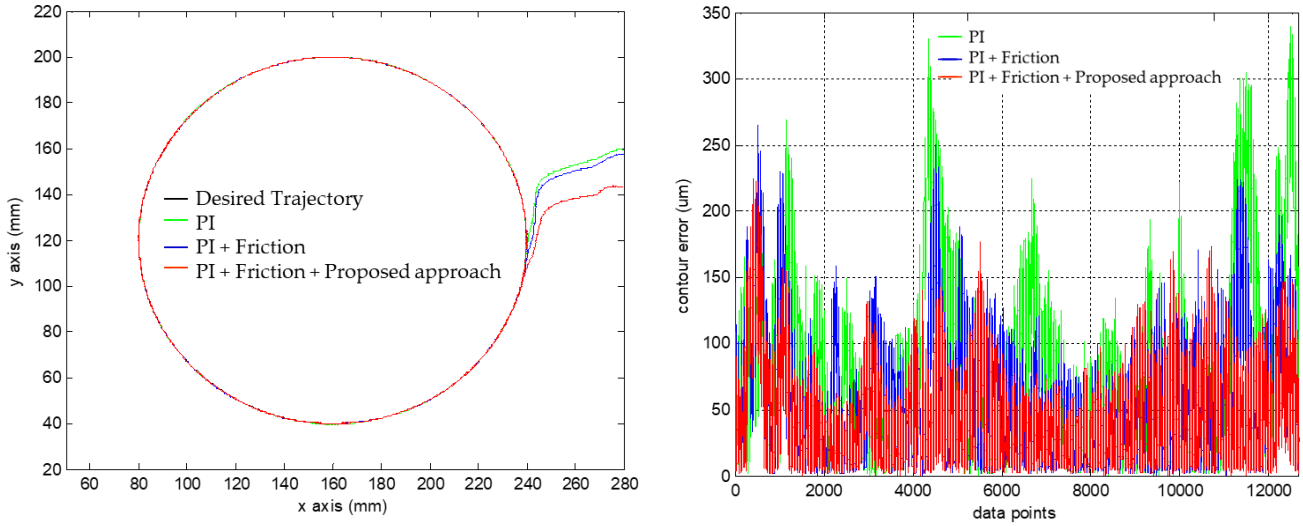

(a) (b)

FIGURE 6: The Experimental Result. (A) Circle-Shaped Trajectory Tracking (B) Comparisons of Contour Error Among Different Control Schemes.

Fig.6 (a) shows the experimental result of the circle-shaped trajectory tracking task, where the black line is the desired circle-shaped contour; the green line is the actual trajectory obtained using PI controller (PI) only; the blue line is the actual trajectory obtained using PI and friction compensation (PI+Friction); the red line is the actual trajectory obtained using the combinations of the PI, friction compensation, and proposed approach (PI+Friction+Proposed approach). The contour errors of the trajectory tracking task resulting from different controller schemes are shown in Fig. 6 (b). In addition, performance indices in terms of root mean square of contour error (RMS), average of integral of absolute contour error (AIAE), and maximum contour error (MAX) are listed in TABLE 3. The results shown in Fig. 6 and TABLE 3 indicate that the PI+Friction+Proposed approach yield the best performance among all the tested control schemes. We have also come up with several interesting observations from Fig. 6. Although PI+Friction can reduce the protrusion error occurring in a reverse motion, its ability in contour error reduction is not so impressive. One of the major reasons is that the LuGre model based friction compensation is mainly used

to cope with the friction force rather than disturbance suppression, and the modeling uncertainty of the LuGre friction model is inherently existed in the identification process and the model parameter variations are frequently occurred in practice. In contrast, using the proposed approach combined with PI+Friction can significantly improve the contour error by reducing the adverse effects of the LuGre friction model inaccuracy.

TABLE 3
PERFORMANCE EVALUATION OF THE CIRCLE-SHAPED TRAJECTORY TRACKING TASK

Definitions	Performance index of contour error		
	AIAE (μm)	RMS (μm)	MAX (μm)
PI	80.18	103.63	340.01
PI+Friction	57.67	74.23	265.69
PI+Friction+proposed approach	44.29	57.23	225.32

V. CONCLUSION

The proposed approach of this study is based on the open-loop disturbance observer adopts the projection type adaptive law to adjust the observer gain. The error between the output of the actual plant and the output of the nominal plant converges to zero asymptotically. Moreover, the robust design utilizes the backstepping algorithms to enhance the performance of disturbance compensation. Additionally, the simulation example of the velocity control on a motor is used to describe the performance of the proposed approach compared with the conventional DOB, and the experiment of the trajectory tracking task has been conducted to verify the abilities of the proposed approach. The results of the simulation and experiment show the satisfactory performance.

ACKNOWLEDGEMENTS

The author would like to thank the Energy Administration, Ministry of Economic Affairs, Taiwan, R.O.C., for supporting this research.

REFERENCES

[1] W.-H. Wang, J. Yang, and S. Li, "Disturbance-observer-based control and related methods-An overview," IEEE Trans. Ind. Electron., vol. 63, pp. 1083-1095, 2016.

[2] C. Liu, J. Wu , J. Liu, and Z. Xiong, "High acceleration motion control based on a time-domain identification method and the disturbance observer," Mechatron., vol. 24, pp. 672-678, 2014.

[3] M. Jouili, K. Jarray, Y. Koubaa, and M. Boussak, "Luenberger state observer for speed sensorless ISFOC induction motor drives," Electr. Power Syst., vol. 89, pp. 139-147, 2012.

[4] C. Peng, J. Fang, and X. Xu," Mismatched disturbance rejection control for voltage-controlled active magnetic bearing via state-space disturbance observer," IEEE Trans. Power Electron., vol. 30, pp. 2753-2762, 2015.

[5] H. D. Rojas, J. and J. Cortes-Romero," On the equivalence between generalized proportional integral observer and disturbance observer," ISA Trans., vol. 133, pp. 397-411, 2023.

[6] J.Q. Han, "From PID to active disturbance rejection control," IEEE Trans. Ind. Electron. , vol. 56,pp. 900-906, 2009.

[7] X. Hou, H. Xing, S. Guo, H. Shi, and N. Yuan, "Design and implementation of a model predictive formation tracking control system for underwater multiple small spherical robot," Appl. Sci., vol. 14, pp. 294, 2004.

[8] Y. Yao, Z. Jiao, and D. Ma, "Adaptive robust control of DC motors with extended state observer," IEEE Trans. Ind. Electron., vol. 61, pp. 3630-3637, 2014.

[9] W.-D. Chang, R.-C. Hwang, and J.-G. Hsieh, "A self-tuning PID control for a class of nonlinear systems based on the Lyapunov approach," J. process control, vol. 12, pp. 233-242, 2002.

[10] S. M. Ghamari, F. Khavari, and H. Mollaee, "Lyapunov-based adaptive PID controller design for buck converter," Soft Computing, vol. 27, pp. 5741-5750, 2023.

[11] J. Lee, P. H. Cheng, B. Yu, and M. Jin, "An adaptive PID control for robot manipulators under substantial payload variations. IEEE Access, vol. 8, pp. 162261-162270, 2020.

[12] G. Tao, "Adaptive control design and analysis," Wiley, NJ, USA, 2003.

[13] M. Krstic, L. Kanellakopoulos, and P. V. Kokotovic, "Nonlinear and adaptive control design" Wiley, NY, USA, 1995.

[14] J. J. E. Slotine and W. Li, "Applied nonlinear control," Prentice-Hall, NJ, USA, 1991.

[15] C. Canudas de Wit, H. Olsson, K. J. Astrom, and P. Lischinsky, "A new model for control of systems with friction," IEEE Trans. Autom. Control, vol. 40, pp. 419-425, 1995.

[16] M. R. Kermani, R. V. Patel, "Moallem, M. Friction identification and compensation in robotic manipulators," IEEE Trans. Instrum. Meas., vol. 56, pp. 2346–2353, 2007.

AD Publications
Sector-3, MP Nagar, Bikaner,
Rajasthan, India
www.adpublications.org, info@adpublications.org